ACS APPLIED MATERIALS & INTERFACES

www.acsami.org Research Article

# Wearable Strain Sensors Using Light Transmittance Change of Carbon Nanotube-Embedded Elastomers with Microcracks

Jimin Gu, Donguk Kwon, Junseong Ahn, and Inkyu Park*

Cite This: ACS Appl. Mater. Interfaces 2020, 12, 10908−10917 Read Online

ACCESS | Metrics & More | Article Recommendations | Supporting Information



**ABSTRACT:** A number of flexible and stretchable strain sensors based on piezoresistive and capacitive principles have been recently developed. However, piezoresistive sensors suffer from poor long-term stability and considerable hysteresis of signals. On the other hand, capacitive sensors exhibit limited sensitivity and strong electromagnetic interference from the neighboring environment. In order to resolve these problems, a novel stretchable strain sensor based on the modulation of optical transmittance of carbon nanotube (CNT)-embedded Ecoflex is introduced in this paper. Within the film of multiwalled CNTs embedded in the Ecoflex substrate, the microcracks are propagated under tensile strain, changing the optical transmittance of the film. The proposed sensor exhibits good stretchability ($\varepsilon \approx 400\%$), high linearity ($R^2 > 0.98$) in the strain range of $\varepsilon = 0-100\%$, excellent stability, high sensitivity (gauge factor ≈ 30), and small hysteresis (∼1.8%). The sensor was utilized to detect the bending of the finger and wrist for the control of a robot arm. Furthermore, the applications of this sensor to the real-time posture monitoring of the neck and to the detection of subtle human motions were demonstrated.

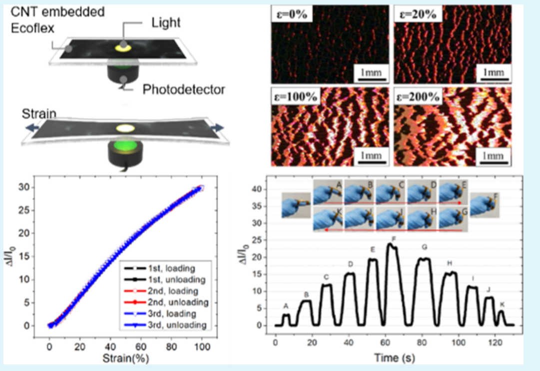


**KEYWORDS:** *optical strain sensor, stretchable sensor, carbon nanotube, wearable sensor, elastomer composite*

## INTRODUCTION

Recently, stretchable and flexible strain sensors are considered as very useful components for the wearable healthcare and human−machine interface systems. For human motion detection, mechanical flexibility, linearity, sensitivity, stability, and dynamic range of the sensors should be sufficient.[1−7] In order to satisfy these requirements, various stretchable strain sensors based on the nanomaterial−polymer composite have been developed. For example, polymer composites with silver nanowires,[8−10] silver nanoparticles,[11,12] graphene,[13,14] and carbon nanotubes (CNTs)[15−20] have been utilized as the functional nanomaterials for the stretchable strain sensors. Especially, CNTs are widely used as a functional nanomaterial for the strain sensors because of their good mechanical and electrical characteristics[21] and thermal stability.

Most research on the strain sensors with CNTs as a functional nanomaterial has been based on the piezoresistive or piezocapacitive transduction mechanisms by the external strain.[19,22,23] Previously, a dual-layer structure composed of the CNT film and elastomer substrate and the CNT−elastomer mixture composite structure have been used as strain-sensing materials. Among them, some piezoresistive strain sensors have shown high stretchability ($\varepsilon \approx 500\%$), high sensitivity, and easy integration for practical applications. For piezoresistive sensors, sensor performances can be improved by modulating the characteristics of the elastomer composite with single-walled CNTs or multiwalled CNTs (MWCNTs).[15−19,24,25] More recently, improvement of stretchability and sensitivity was suggested by applying a core−shell structure using CNT.[24,25] With these efforts, some piezoresistive strain sensors have shown a high gauge factor (GF > 20), but they have suffered from poor linearity in the high strain region ($\varepsilon \approx 100\%$).[18,26] Moreover, poor stability and high sensitivity to the temperature and humidity have been common problems of the pizeoresistive sensors. On the other hand, piezocapacitive strain sensors based on the CNT−elastomer mixture composite have shown better stability, lower hysteresis, and high stretchability ($\varepsilon \approx 500\%$).[22] However, the piezocapacitive-type strain sensors have GFs relatively lower than those of the piezoresistive-type sensors and are highly influenced by the surrounding conductive objects because of the electromagnetic interference.

The optical-type strain sensor can be a good alternative to resolve the abovementioned limitations of piezocapacitive and piezoresistive strain sensors because they are less affected by the environmental disturbances. Recently, an optical-type strain sensor based on the change of optical transmittance of the

Received: October 5, 2019
Accepted: December 26, 2019
Published: December 26, 2019

titanum oxide ($TiO_2$)−Ecoflex composite has been introduced.[27] The sensor was composed of a light detector, a light source, and a $TiO_2$−Ecoflex composite between them, showing a high stretchability ($\varepsilon \approx 500\%$) and a moderate transmittance change (30% change of transmittance for $\varepsilon \approx 500\%$). However, this sensor exhibited a low GF (∼3.1), and critical sensing performances such as dynamic response, limit of detection, hysteresis, strain rate dependence, and reproducibility of the sensor are not presented in this article. Furthermore, only a limited application such as finger-bending motion detection was demonstrated.

In this paper, we introduce an optical-type stretchable strain sensor based on the change of optical transmittance of the CNT-embedded Ecoflex film. In order to achieve a large dynamic range of the sensor, we chose Ecoflex as an elastomeric substrate with low Young's modulus ($E \approx 125$ kPa), good mechanical durability, flexibility, and attachability on the human skin. MWCNTs were spray-coated and embedded into the Ecoflex substrate, and the microcrack propagation in this MWCNT film led to optical transmittance change. We evaluated critical sensing performances of the developed strain sensor such as sensitivity, linearity, dynamic characteristics, hysteresis, stability, and reproducibility. It showed good stretchability ($\varepsilon \approx 400\%$), high linearity ($R^2 > 0.98$), excellent stability, high sensitivity (GF ≈ 30), and small hysteresis (∼1.8%). The sensor responses were observed to be independent on the intensity of the light source and strain rate. The sensor was utilized to detect the bending of the finger and wrist for the control of the robot arm. Furthermore, the applications of this sensor to the real-time monitoring of neck posture, carotid pulse, and face expression were demonstrated.

## EXPERIMENTAL SECTION

**Fabrication of the CNT-Embedded Ecoflex Thin Film, Pristine Ecoflex, and CNT−Ecoflex Mixture Composite.** First, CNTs (Hanwha Chemical, Republic of Korea) were mixed with isopropyl alcohol (0.025 wt %) and spray-coated on the donor substrate [poly(ethyl benzene-1,4-dicarboxylate), PET Petri dish]. The coating density was controlled by measuring the sheet resistance of deposited CNT film. The Ecoflex prepolymer (Smooth-On, Inc., USA) was prepared by mixing it with a curing agent at a weight ratio of 1:1. It was first poured on the donor substrate that was already coated with CNTs and then was cured at room temperature (25 °C) for 3 h. As a result, the CNTs were embedded into the Ecoflex substrate. After curing, the CNT-embedded Ecoflex was detached from the donor substrate (Figure S1).

The pristine Ecoflex and CNT−Ecoflex mixture composite were used to compare the performance of the strain sensor. In order to make the pristine Ecoflex, the prepolymer mixture with a curing agent (1:1 weight ratio) was poured on the donor substrate (PET Petri dish) and then cured at room temperature (25 °C) for 3 h. In order to make the CNT−Ecoflex mixture composite, CNTs were added on the Ecoflex prepolymer mixed with a curing agent at a weight ratio of 1:1. CNTs and Ecoflex were mixed using a planetary mixer for 2 min. The amount of the CNT ratio is 0.52 wt % which is the same amount of the CNT density with sheet resistance 78.9 Ω/□ of the CNT-embedded Ecoflex. After pouring on the donor substrate (PET Petri dish), bubbles were removed using a vacuum chamber. After curing at room temperature for 3 h, the CNT−Ecoflex mixture was removed from the donor substrate.

**Measurement System.** As a light source to characterize the sensor performance, a solar illuminator (LAX-C100 Xenon light source, Asahi Spectra Co., Ltd., Inc., Japan) with a visible range ($\lambda$ = 400−800 nm) was employed (Figure S2). The intensity of the light transmitted through the CNT-embedded Ecoflex thin film was measured using a photodiode (PD) power sensor (S120C, Thorlabs, Inc., USA) with a universal serial bus power and energy interface (PM100USB, Thorlabs, Inc., USA). The tensile strain was applied in a customized linear stage. The optical characteristics of CNT-embedded Ecoflex thin film were examined using a UV−vis spectrometer (Lambda 650, PerkinElmer, Inc., USA). Before characterization, fabricated CNT-embedded Ecoflex thin film was tested under the conditions of about 10% initial strain after 200% prestrain.

In order to evaluate the sensor performance under harsh environmental conditions, especially in different humidity conditions, the whole space was sealed using the polyvinyl plastic to maintain particular relative humidity using a humidifier. The humidity of the space was measured using a commercial humidity sensor (A13T, Uni-Trend Technology Co., Ltd. China).

For a high-temperature experiment, the CNT-embedded Ecoflex was attached to a slide glass and hung within a convection oven for 72 h. The length of the CNT-embedded Ecoflex thin film was measured after 1, 2, 3, 5, 12, 24, and 72 h. The load (weight = 50 and 200 g) was hung at the edge of the Ecoflex, and the fine pin was fixed for the length measurement with a metal ruler.

**Thermal Characteristics of the Ecoflex.** The thermal characteristics of Ecoflex 0030 were examined using differential scanning calorimetry (DSC, 214 Polyma, NETZSCH, Germany) and thermogravimetric analysis (TGA, TG209 F1 Libra, NETZSCH, Germany). For each analysis, the Ecoflex 0030 agents A and B were mixed in a 1:1 weight ratio and cured at $T$ = 100 °C for 3 h. DSC analysis was conducted using a sample mass of 8.301 mg at the temperatures from 20 to 200 °C in a $N_2$ environment. TGA was conducted using a sample mass of 7.661 mg at temperatures from 30 to 700 °C in a $N_2$ environment.

**Image Analysis.** The photographs taken using the charge-coupled device (CCD) camera were converted into 8 bit gray tone images, and each image was set to the same intensity to calculate the area of the bright part that increased with microcrack opening by the applied tensile strain (Figure S3).

**Strain Sensor Package for Human Motion Detection.** A light-emitting diode (LED) and PD (i.e., photodetector) were integrated with the CNT-embedded Ecoflex thin film for sensor packaging (Figure S4). A chip LED (5550 SMD LED, peak wavelength $\lambda$ = 520 nm, ITSWELL, Inc., Republic of Korea) and a surface mount device-type PD (TEMD6010FX01, Vishay, Inc., USA) embedded in the Ecoflex film were attached on the upper and lower sides of CNT-embedded Ecoflex thin film, respectively. The LED and PD were embedded in the Ecoflex by placing them in a 3D-printed thermoplastic polyurethane mold with a dimension of 50 mm × 15 mm × 2 mm, followed by pouring the Ecoflex prepolymer and curing at 60 °C. Each side of the LED- and PD-embedded Ecoflex was attached with the CNT-embedded Ecoflex thin film with a silicone adhesive (Sil-Poxy, Smooth-On, Inc., USA). The total thickness of the strain sensor package was less than 5 mm. A single-axial strain sensor package was utilized for the detection of finger and wrist motions, neck pulses, uvula swallowing, and face expression. A triaxial strain sensor package for neck posture monitoring was also fabricated by the same method. When the direction parallel to the cervical vertebral is assumed to be 0°, an array of three strain sensors with an angle of 0, −15, and +15° for each sensor was fabricated.

**Measurement System of Human Motion Detection.** The LED of the strain sensor package was connected with a power supply with a bias voltage of 3 V. For a single-axial strain sensor package, the PD was connected with a source meter (Keithley 2400, Tektronix, Inc., USA) that was controlled by LabVIEW program (National Instruments, USA) to measure the real-time current in a reverse bias mode (bias voltage = −0.1 V). For each human motion detection, each end of the strain sensor package was attached on the skin. A triaxial strain sensor package for the neck posture monitoring was also fixed with a medical double-sided tape. In particular, the root of the sensor was attached on the location of the cervical vertebral. For a triaxial strain sensor package, each PD was connected with an operating amplifier to convert the current signal to the voltage signal. The voltage output was measured by Arduino UNO, which can measure more than three channels simultaneously in real-time.



https://dx.doi.org/10.1021/acsami.9b18069
ACS Appl. Mater. Interfaces 2020, 12, 10908−10917

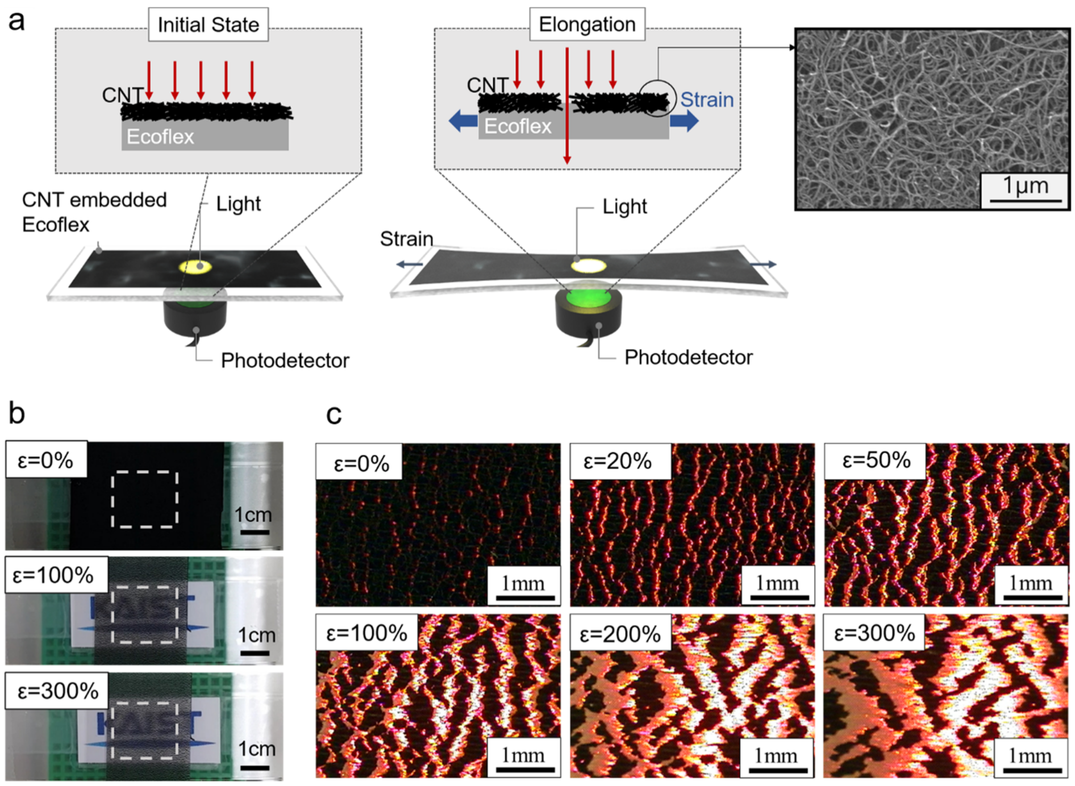


**Figure 1.** Principle and mechanism of the CNT-embedded Ecoflex thin film-based strain sensor: (a) schematic of the sensor based on the optical transmittance change of the CNT-embedded Ecoflex thin film because of the microcrack opening of the CNT network and the scanning electron microscopy image of spray-coated CNTs, (b) photographs of the optical transmittance change of CNT-embedded Ecoflex thin film by the applied tensile strain, and (c) CCD camera image of the microcrack generation and propagation in the CNT-embedded Ecoflex thin film under increasing tensile strain.

**Control of the Robot Arm by Finger and Wrist Motion Detection.** For controlling the robot arm using the designed sensor, a source meter and PD were replaced with Arduino UNO REV3 and the cadmium sulfide (CdS) cell (GL3526 CdS, Cosocomy, Inc., China), respectively, to simplify the data acquisition and motion control of the robot arm. A voltage divider circuit with a serial connection of a variable resistor (i.e., CdS cell) and a fixed resistor and a constant 5 V voltage supplied from Arduino was utilized. The Arduino board was used to provide power (bias voltage = 5 V) to the LED and to read the voltage change by the light intensity change from the CdS cell. A robot gripper and a wrist motor were connected with the Arduino digital control pin for motion control, and a 9 V battery was used for the power supply. In the Arduino code, the human finger and wrist movements were converted to the motor control values of the robot gripper and the robot wrist, respectively.

## ■ RESULTS AND DISCUSSION

Figure 1a describes the principle of the proposed sensor. The external strain applied to the Ecoflex transfers to the embedded CNTs, generating microcracks that are propagated in proportion to the applied strain. A light source and a photodetector are installed on the upper and lower sides of the CNT-embedded Ecoflex thin film, respectively. Before the microcrack generation, the light transmission through the CNT-embedded Ecoflex thin film is very low because of the absorbance and scattering of the incident light by the embedded CNTs. When the microcrack is generated by the applied strain, light can pass through the microcrack opening, and therefore, the optical transmittance of the CNT-embedded Ecoflex thin film increases as shown in Figure 1b. Initially, on a zero strain, the background letter was completely blocked by the CNT-embedded Ecoflex thin film. As the external strain is increased, the optical transmittance of CNT-embedded Ecoflex thin film is increased and thereby the background letter gradually appears. Figure 1c displays the images of the microcrack generation and propagation corresponding to the external strain that is captured using a CCD camera. In this figure, the bright side of the image is Ecoflex that transmits the incident light. As the applied strain is increased, more microcracks are generated and further propagated, which opens the path for the light transmission.

The optical transmittance change of the CNT-embedded Ecoflex thin film by the applied strain ($\varepsilon = 0-100\%$) is depicted in Figure 2a. The output response is defined as $\Delta I/I_0$, in which $I_0$ and $\Delta I$ represent the initial light intensity and the change in the light intensity through the CNT-embedded Ecoflex thin film, respectively. The transmittance is the effectiveness of light transmission, which is defined as the ratio of the light intensity passing through the medium to the original intensity of the incident light. From this relationship, the ratio of the light intensity change to the initial light intensity represents the relative transmittance change of the medium. The responses in loading and unloading cycles show negligible hysteresis. Here, the hysteresis is defined by the ratio of the midpoint gap between the loading and unloading curves to the gap between the minimum and maximum output values. It is shown that almost complete recovery is achieved with an error of 1.9%, and the hysteresis is as low as 1.8% for three loading cycles. Also, the sensor response to the applied strain can be approximated as a linear function with $R^2$ = 0.997. As mentioned above, the proposed sensors were first prestrained by 200% after they were fabricated. By this prestretching process, most of the initial



https://dx.doi.org/10.1021/acsami.9b18069
ACS Appl. Mater. Interfaces 2020, 12, 10908−10917

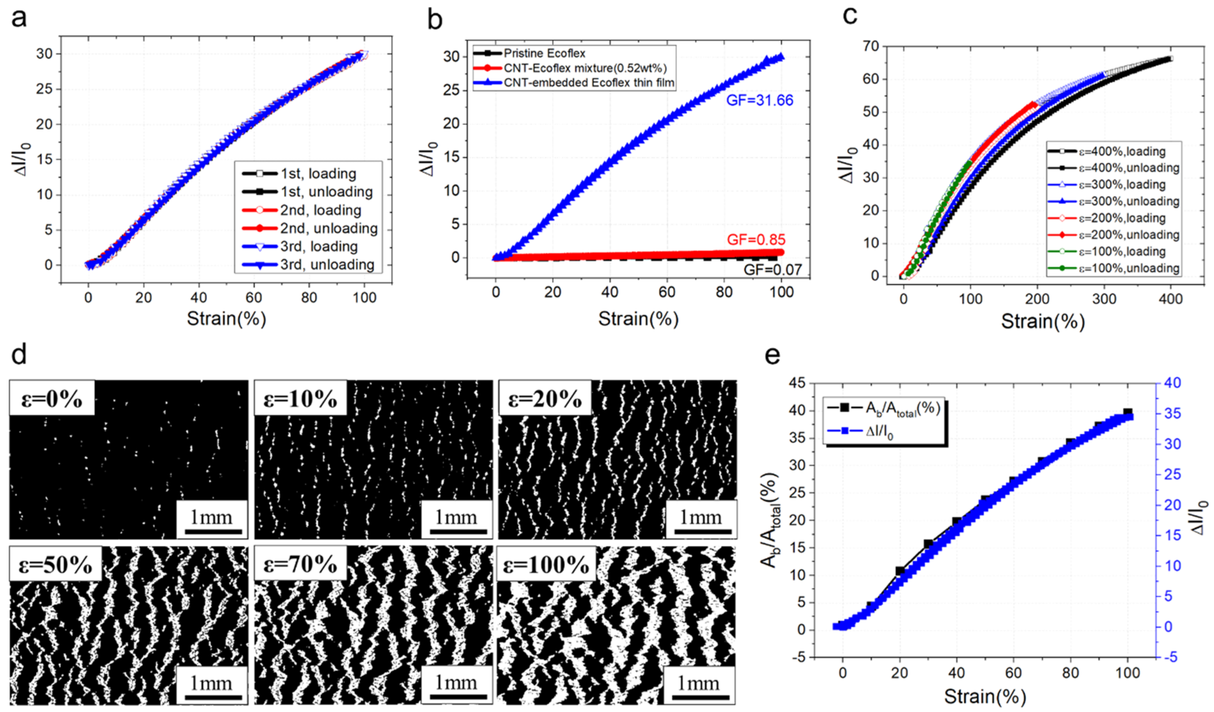


**Figure 2.** Performance characterization of the CNT-embedded Ecoflex thin film-based strain sensor: (a) input strain vs output sensor signal, (b) comparison of the sensor performances of the pristine Ecoflex, CNT−Ecoflex mixture (CNT concentration = 0.52 wt %), and the proposed CNT-embedded Ecoflex thin film, (c) loading−unloading curves of the strain sensor for $\varepsilon$ = 100−400% strains, (d) image analysis of photos of the sensor under strains of $\varepsilon$ = 0−100% taken using a CCD camera, (e) comparison of the image analysis result (i.e., relative change of the bright area) and the sensor response (i.e., relative change of the light intensity that is transmitted through the sensor) under strains of $\varepsilon$ = 0−100%. Here, $A_b$ and $A_{total}$ represent the bright area (with microcrack opening) and the total area in Figure 2d, respectively. $\Delta I$ and $I_0$ indicate the light intensity change and the light intensity on a zero strain through the sensor, respectively.

cracks were generated before the performance characterization and application of the sensors. Therefore, crack opening and closure occur from initially formed cracks, where tensile stress is concentrated. This enables quick and complete recovery of crack dimensions. In the case of piezoresistive sensors based on the nanomaterial−elastomer composites, the recovery of Ohmic contact between nanomaterial fillers should take place when the strain is released, which results in the hysteresis.[8] In contrast, in our sensor, as long as the crack dimensions are recovered, the optical transmittance is immediately recovered. We presume that this would be the reason for the negligible hysteresis of our sensor.

Figure 2b compares the responses of the CNT-embedded Ecoflex thin film, pristine Ecoflex, and CNT−Ecoflex mixture composite to the applied tensile strain in the range of $\varepsilon$ = 0−100%. The GFs of the pristine Ecoflex and CNT−Ecoflex mixture composite are GF = 0.07 and GF = 0.85, respectively. In the case of the CNT−Ecoflex mixture composite, it has been reported that their stretching results in the rearrangement of the CNT filler inside the elastomer matrix.[28,29] Here, the crack opening does not occur but only the rearrangement of CNTs happens, thereby no significant change of optical transmittance is generated. On the other hand, CNT-embedded Ecoflex thin film shows a much larger GF (GF = 31.66). This phenomenon can be attributed to the large transmittance change caused by the amount of light passing through the microcracks generated by the strain, which is explained in detail later.

There are some factors that affect the response of the proposed sensor. As mentioned above, the response of the sensor is defined by the ratio of the light intensity change to the initial light intensity that transmits through the CNT-embedded Ecoflex thin film. The light intensity is determined by the optical transmittance of the film. Therefore, the initial light transmittance affects the sensitivity of the sensor. The initial CNT coating density and the prestrain on the CNT-embedded Ecoflex thin film are dominant factors to determine the initial light transmittance. The initial CNT coating density is indirectly evaluated by the sheet resistance of the spray-coated CNT random network. The sheet resistance decreases when the density of the CNT film increases (Figure S5a). Because of this reason, the initial light transmittance decreases when the sheet resistance is lower (Figure S5b). As a result, the GF of the sensor increases from 5 to 175 when the sheet resistance was decreased from 650 to 40 Ω/□ (Figure S5c). However, when the sheet resistance was smaller than 40 Ω/□, spray-coated CNT film did not get fully embedded in the Ecoflex substrate, which causes the delamination of CNTs from the Ecoflex (Figure S5d).

In addition, even if the density of the CNT film is identical, the sensor response also depends on the prestrain and initial strain of the CNT-embedded Ecoflex thin film. As shown in Figure S6a, when 50% prestrain was applied and a little microcracks were formed, 100% strain loading−unloading showed high hysteresis (4.6%) because of newly formed microcracks. On the other hand, when 200% prestrain was applied, much smaller hysteresis (1.5%) was observed. This is because most crack opening occurs from the initially formed cracks by 200% prestrain, and new cracks are rarely generated in other locations. For the sensor characterization and applications, we have applied small positive initial strains in order to obtain stable sensor signals. Here, the degree of the initial strain is defined as $\varepsilon_i = (L_i - L_0)/L_0$ and the applied strain is defined as $\varepsilon = (L - L_i)/L_i$, in which $L_0$ and $L_i$ represent the original length of the CNT-


https://dx.doi.org/10.1021/acsami.9b18069
ACS Appl. Mater. Interfaces 2020, 12, 10908−10917

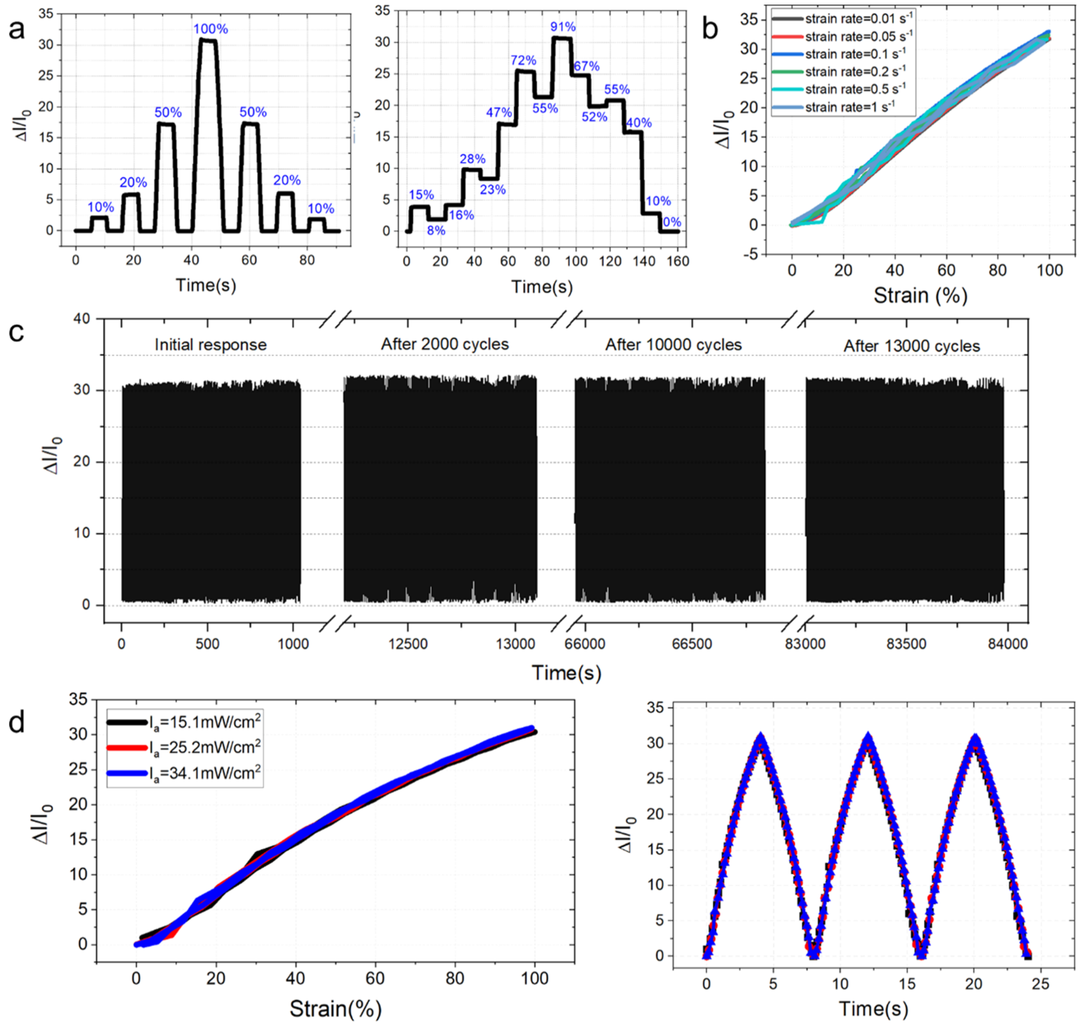


**Figure 3.** Dynamic characteristics of the CNT-embedded Ecoflex thin film-based strain sensor: (a) sensor response to various input strains between $\varepsilon$ = 0 and $\varepsilon$ = 100%, (b) sensor response to different input strain rates (strain rate = 0.01, 0.05, 0.1, 0.2, 0.5, and 1 $s^{-1}$), (c) durability test for 13,000 cycles of $\varepsilon$ = 0−100%, and (d) effect of the initial light intensity on the sensor response; the response of the sensor is independent to the initial light intensity from the light source.

embedded Ecoflex film and the length when it was fixed on the linear stage, respectively. As the initial strain increases, initial light transmittance through the CNT-embedded Ecoflex film increases and thus GF decreases (Figure S6b,c). Figure 2c shows the sensor response in the loading and unloading cycles for the strain larger than $\varepsilon$ = 100%. Using the Ecoflex as a base material, the dynamic range is as wide as $\varepsilon \approx$ 400%. The hysteresis of the sensor is 1.8% for the strain range of $\varepsilon$ = 0−100%, whereas 7.6% for the strain range of $\varepsilon$ = 0−400% (Table S1). Also, the linearity of the sensor worsens when the strain range is increased. This can be explained by the mechanism of light transmittance change through the film. When the initial strain is applied within the area of the photodetector, the light transmittance changes as a result of the formation of microcracks between the CNTs. However, if the stretching exceeds a certain range, the amount of additional microcrack formation decreases and the increasing rate of light transmittance is reduced. The reason of this phenomenon is due to a large Young's modulus difference between MWCNTs (a few GPa[30]) and Ecoflex (∼125 kPa). By initial stretching, cracks are randomly generated and propagated in the MWCNT film. If more strain is applied because of the large Young's modulus difference between the Ecoflex and MWCNT film, no new cracks are generated and stretching occurs only in the Ecoflex region. The crack opening can be simply modeled as shown in Figure S7a. Here, $L_A$ and $L_B$ represent the lengths of transparent (i.e., Ecoflex) and opaque (i.e., MWCNT) regions, respectively. The optical transmittance in the model could be represented as $L_A/(L_A + L_B)$. As more strain is applied, most change occurs in $L_A$, while the change in $L_B$ is much less because of the reason explained above (i.e., large difference of stiffness between Ecoflex and MWCNTs). This optical transmittance value converges to 1 with decreasing slopes by applying larger strain as shown in Figure S7b.

Figure 2d,e shows the change in light transmittance of the film by the area of bright (i.e., optically transparent) regions in the optical microscope image. In Figure 2d, the black and white regions represent the opaque area covered by the CNTs and the transparent area because of the microcrack opening. In Figure 2e, the changes of the transparent area and intensity of transmitted light by applying tensile strain are presented. Two graphs show almost identical relations to the applied strain, which interprets that the increase of the microcrack opening is the dominant principle for the change of the light transmittance of the CNT-embedded Ecoflex thin film. The high sensitivity of the sensor could be explained by this microcrack propagation mechanism.



https://dx.doi.org/10.1021/acsami.9b18069
ACS Appl. Mater. Interfaces 2020, 12, 10908−10917

The dynamic characteristics of the proposed strain sensor are shown in Figure 3. Figure 3a shows the response to various strain inputs from $\varepsilon$ = 0% to $\varepsilon$ = 100%. The sensors showed good response and recovery characteristics to various strain inputs. Figure 3b compares the sensor responses for different strain rates. The experimental data represent the independence of the sensor response to the strain rate in the range of $d\varepsilon/dt$ = 0.01−1 $s^{-1}$. For each strain rate, hysteresis was calculated and is listed in Table S2. Below the strain rate of 0.2 $s^{-1}$, the hysteresis is under 2%. Above the strain rate of 0.5 $s^{-1}$, the motor was overloaded and thus its vibration caused the error of the sensor response. However, even in this case, the calculated hysteresis is still under 5.5%. Figure 3c shows the durability of the sensor for 13,000 cyclic loading of $\varepsilon$ = 0−100%. As shown in the graph, in the initial cyclic loading, the response after 2000 and 10,000 sets of cyclic loading and the response after 13,000 sets of cyclic loading are stable without any noticeable drift. This suggests that the sensor response can be used without degradation even if the sensor is repeatedly used for a long time period. The reason of poor stability of previously reported piezoresistive strain sensors is the loss of electrical connections because of external strain loading−unloading, as mentioned in the literature.[31] In the proposed sensor, microcrack formation is quantified by measuring the optical transmittance, and thus, electrical connection loss between the nanomaterials would not affect the performance of the sensor. In addition, in our sensor, the uncured Ecoflex prepolymer permeated through the CNT network, forming a physical entanglement between CNTs and Ecoflex, resulting in a stable attachment. Although van der Waals bonding exists between the surfaces of CNTs and Ecoflex, mechanical interlocking between them due to complex entanglement enables their strong physical bonding. The effect of intensity of the light source to the sensor characteristics is shown in Figure 3d. It can be seen that the sensor response is consistent regardless of the initial light intensity. As explained in the section "independency of the sensor response to the intensity and wavelength of the light source" of the Supporting Information, the sensor response ($\Delta I/I_0$) depends on the transmittances of the pristine Ecoflex ($T_{\mathrm{Ecoflex}}$) and CNT-embedded Ecoflex ($T_{\mathrm{CNT}}$) and the fraction of the pristine Ecoflex ($f_{\mathrm{Ecoflex}}$) due to the microcrack opening by the applied strain. As shown in Figure S8, $T_{\mathrm{Ecoflex}}$ and $T_{\mathrm{CNT}}$ are almost constant regardless of the intensity of the incident light. Therefore, the sensor response is only dependent on the applied strain and is not affected by the incident light intensity. The effect of the wavelength of the light to the sensor characteristics is shown in Figure S9. In the visible range ($\lambda$ = 460−620 nm), the sensor characteristic is independent of the wavelength.

The mechanism of the sensor is the transmittance change of the CNT-embedded Ecoflex film due to the opening of microcracks by applied strain. Thus, the homogeneity of the microcrack formation in the CNT film is important to achieve the uniformity of the sensing performance and it was observed by comparing the sensor responses for different positions of the photocouple (i.e., a pair of a LED and PD) (see Figure S10). For a 45 mm long sample, The LED and PD photocouple was positioned at two different locations ($x$ = 0 and 10 mm with respect to the center). As shown in Figure S10b, there was no significant difference in the sensor performance by changing the sensing locations. This can be explained by the uniform microcrack opening throughout the sensor. As shown in Figure S10c, the relative change of the microcrack opening area under applied strain was almost identical for $x$ = 0 and 10 mm. The numerical simulation result of the strain distribution on Ecoflex when a bilateral strain was applied along the $x$-axis reveals that the strain is almost uniform with a maximum error of ±5% in the region of $|x| \leq 15$ mm with respect to the center of the sample (see Figure S10d,e; detail of numerical simulation modeling is provided in the Supporting Information). Therefore, the sensor performances are almost identical at least in the range of $|x| \leq 15$ mm.

The reproducibility of the sensor was investigated by measuring the responses of five different samples in the strain range of $\varepsilon$ = 0−100%. Spray-coated CNT films showed an average sheet resistance of 78.9 Ω/□ with a standard deviation of 6.31 Ω/□ when no strain was applied (i.e., $\varepsilon$ = 0%). As shown in Figure S11a, the sensor responses for five different sensors show good uniformity with a relatively small standard deviation (<10% of the average) for each strain. It is expected that the standard deviation of the sensor results from the variation of CNT film thickness, which is represented by the standard deviation of sheet resistance by 8%. It is expected that the reproducibility can be further improved by a strict control of the fabrication process.

As shown in Figure S11b,c, the smallest strain that the proposed sensor can measure was determined. In Figure S11b, step strain inputs with an increment of 0.03% were applied to the sensor every 10 s. The limit of detection can be defined as three times the signal-to-noise ratio without the input signal divided by the slope of the starting point of the input and output.[32] For six different samples, the limit of detection was calculated using the abovementioned definition which is shown in Table S3, and it turns out to be $\varepsilon_{\mathrm{LOD}}$ = 0.015%.

Figure S12 shows the transient and steady-state responses of the sensor to a step strain input of $\varepsilon$ = 100%. When the strain was maintained at $\varepsilon$ = 100% for 10 min, the drift value defined as the relative change of response of the sensor was as small as 0.8% of its output response, which reveals high stability of the sensor. Figure S13 shows the determination of the response time of the sensor. Here, the sensor was approximated as a first-order system, and the response time could be estimated by the time gap between a ramp strain input and the sensor output. In particular, the time gap when the strain input and sensor response reached 50, 63, and 80% of the steady-state value was utilized to calculate the response time of the sensor for different applied strain inputs (steady-state strains of 10, 20, 50, and 100%). For each strain input, all the response time turned out to be below 50 ms. This result reveals that the sensor has a high response speed and is suitable for many wearable sensing applications that involve quick motions.

Figure S14 shows the harsh environmental effect on the sensor operation. By measuring the sensor response at different relative humidities, we could find that there is no significant influence of relative humidity as shown in Figure S14a. The temperature effect on the sensor performance was investigated by studying the literature on the thermal expansion of Ecoflex 0030[33] and experimentally measuring its long-term thermal creep behavior at an elevated temperature. According to ref 29, the thermal expansion coefficient of Ecoflex 0030 is 284.2 ppm/°C. This means that it will elongate by 2.84% at a temperature increase by 100 °C. In common wearable applications, the temperature rise may not be larger than 20 °C, thereby the thermal expansion is expected to be less than 0.6% and will not disturb the sensor response significantly. Although we have considered Ecoflex only for this calculation, the actual sensor sample (i.e., CNT-embedded Ecoflex) is expected to show a


https://dx.doi.org/10.1021/acsami.9b18069
ACS Appl. Mater. Interfaces 2020, 12, 10908−10917

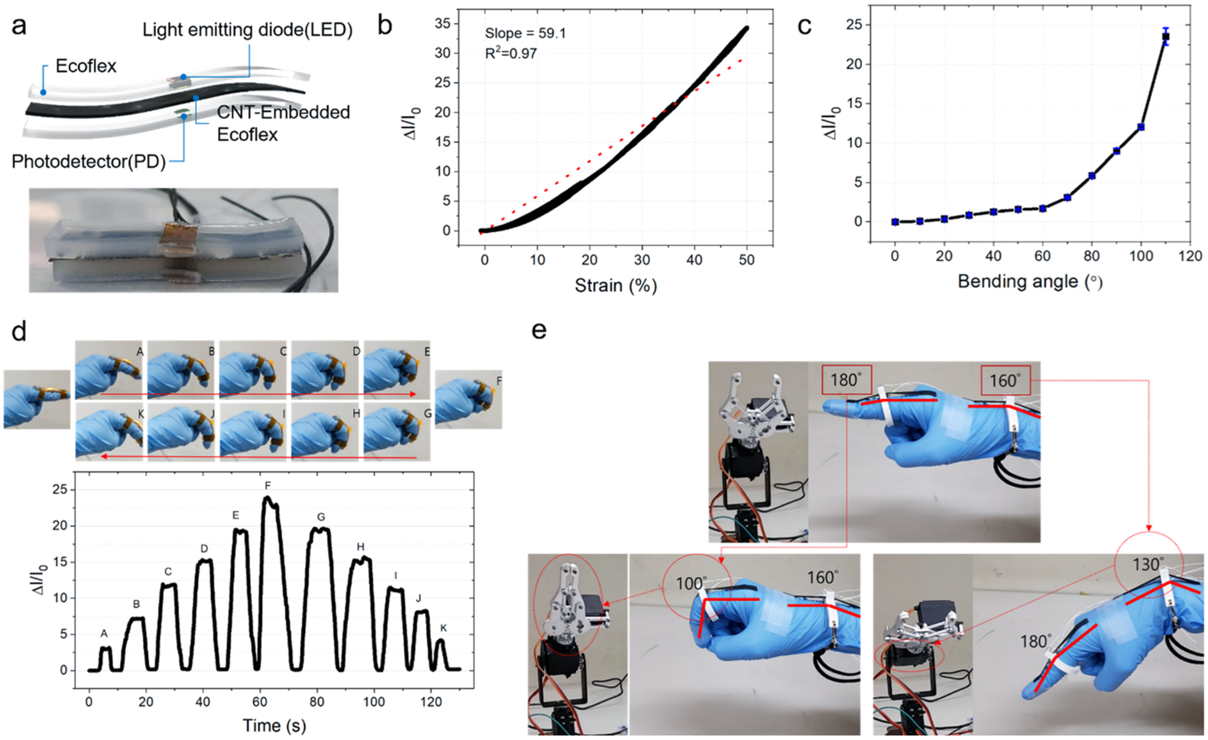


**Figure 4.** Applications of the CNT-embedded Ecoflex thin film-based strain sensor with a photocouple consisting of an LED chip and a photodetector for the human motion detection: (a) schematic image and photo of the strain sensor package, (b) response of the strain sensor package to the uniaxial strain input, which shows a high GF of 70 in the strain range of $\varepsilon$ = 0−50%, (c) response of the strain sensor package to the bending angle, (d) detection of finger-bending motions, and (e) real-time control of the robot gripper and wrist by monitoring the motions of the human finger and wrist.

similar thermal expansion behavior because of the very small thickness of the CNT layer compared to that of the Ecoflex substrate.

In addition, long-term thermal creep characteristics of Ecoflex 0030 were examined under constant loads of 1.96 and 0.49 N at $T$ = 100 and 50 °C for a long time period (Figure S14b,c). When the temperature increased from room temperature to high temperature ($T$ = 100 °C), the strain was quickly reduced as shown in Figure S14b. Under load = 1.96 N at $T$ = 100 °C, the strain decreased from $\varepsilon$ = 108% to $\varepsilon$ = 90%. When a load of 0.49 N was applied at $T$ = 100 °C, the strain decreased from $\varepsilon$ = 41% to $\varepsilon$ = 32.7%. It is presumed that heating caused the volume shrinkage of Ecoflex by evaporating the water molecules that were adsorbed on the Ecoflex (this is explained below with the result of Figure S14d). After this initial strain shrinkage, a slow but gradual strain increase is observed for a long time period because of the creep behavior of Ecoflex. This creep is more obvious when larger loading is applied at higher temperature (e.g., 1.96 N at 100 °C) than when smaller loading is applied at lower temperature (e.g., 0.49 N at 50 °C). The DSC characteristics for two heating cycles shown in Figure S14d reveal that the glass transition did not occur in the temperature range of 20−200 °C. Instead, the difference between the first and second heating processes reflects that water evaporation occurred from Ecoflex during the first heating step. Figure S14e shows the thermal decomposition temperature of the Ecoflex 0030 starting above 200 °C. Therefore, under normal working conditions, within moderate temperature ranges, thermal decomposition of Ecoflex will not be an issue. In summary, there would be a temperature effect to the sensor at high temperatures (i.e., initial volume shrinkage due to water evaporation, followed by a long-term creep deformation). However, for common wearable applications, this high-temperature environment would rarely occur. Therefore, the temperature effect may not be significant for most operation conditions.

Our sensor exhibits a wide dynamic range (0−400%), high sensitivity (GF ≈ 30), and good stability during long-term cyclic loading as shown in Table S4. The capacitive strain sensor has a low sensitivity (GF < 1) because its main mechanism is the geometric change as explained above.[22,34] As compared to the capacitive sensor, the piezoresistive strain sensor exhibits higher sensitivity and linearity but suffers from poor long-term stability under repeated loading.[15] In Zhang, et al.'s work, a vertically aligned CNT−Ecoflex composite-based piezoresistive strain sensor exhibited reduced drifting but the linearity was low and the GF was less than 10.[26] Recently, researchers have reported other strain sensors that exploited 3D-structured or 2D-patterned composite films with silver nanowires or graphene as conductive nanomaterials.[35−38] In their work, localized microcrack formation within 3D structures or 2D patterns significantly increased the sensitivity of the sensor but they still suffered from long-term drift. The optical-type strain sensor based on $TiO_2$ showed a low sensitivity (GF ≈ 3) and its long-term stability was not specified in the work of Zhai and Yang.[27] In contrast, the proposed sensor has a high GF of 31 for $\varepsilon$ = 100%, high linearity ($R^2$ = 0.98), and superior long-term stability for the strain range of $\varepsilon$ = 0−100%.

In order to demonstrate the applicability of our sensor to practical wearable strain-sensing devices, it was employed as (i) human motion-detecting device that measures the finger-bending angle for the robot arm control, (ii) human posture-monitoring device to detect the neck posture, and (iii) subtle human motion-monitoring device to detect human neck pulse, saliva swallowing, and face motion. We demonstrated a human


https://dx.doi.org/10.1021/acsami.9b18069
ACS Appl. Mater. Interfaces 2020, 12, 10908−10917

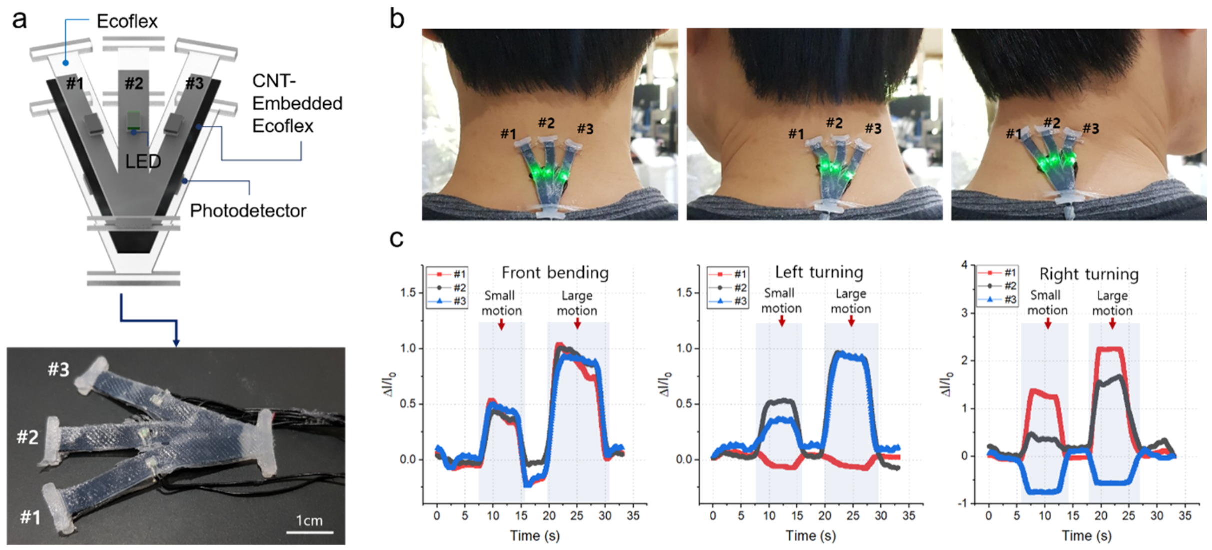

**Figure 5.** Applications of the CNT-embedded Ecoflex thin film-based strain sensor for the human neck posture monitoring with an array of three strain sensor packages: (a) schematic image and photo of the array of three strain sensor packages (CNT-embedded Ecoflex thin film, LED, and photodetector for each sensor package) with an angle of −15, 0, and +15° with respect to the cervical vertebral for each package, (b,c) real-time monitoring of the neck posture that can recognize the neck extension (i.e., front bending), left turn, and right turn with a triaxial strain sensor array.

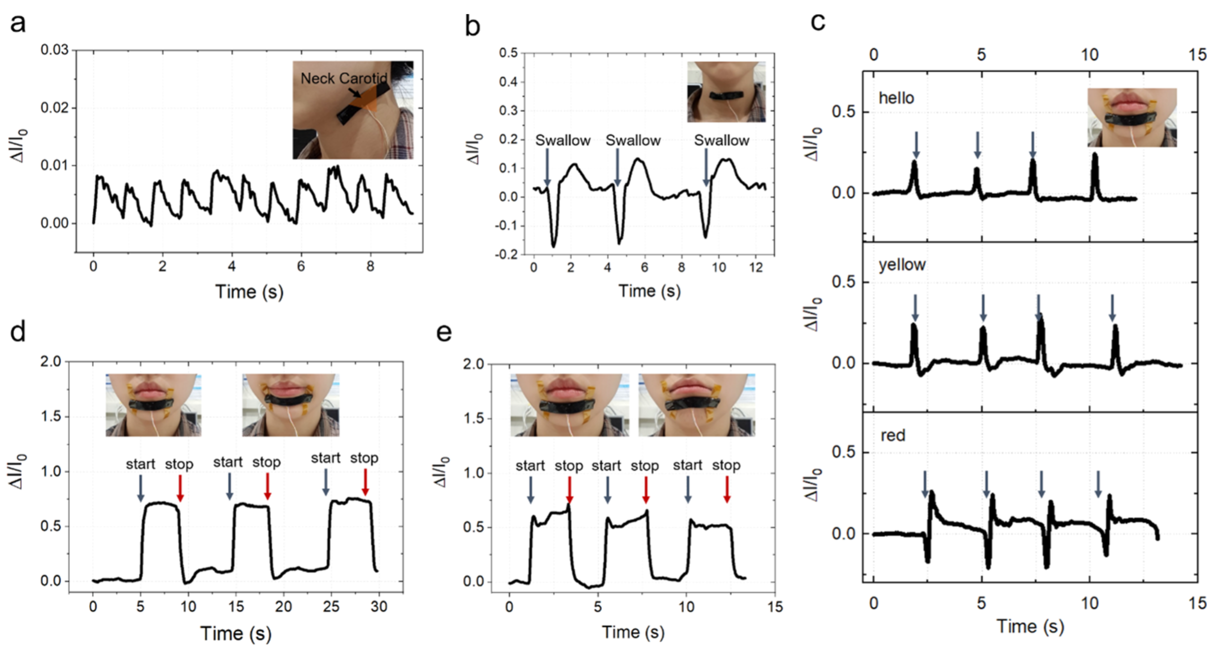

**Figure 6.** Applications of the CNT-embedded Ecoflex thin film-based strain sensor to the monitoring of subtle human motions such as (a) neck carotid pulses, (b) swallowing motion on the uvula, (c) human face expression during speaking different words ("hello", "yellow", and "red"), (d) smiling, and (e) crying.

motion detection device by combining the CNT-embedded Ecoflex thin film and a LED−PD photocouple (Figure 4a). In this strain sensor package, the light emitted from the LED transmits through the CNT-embedded Ecoflex thin film and is detected by the PD underneath. The light transmission through the CNT-embedded Ecoflex thin film is changed by the applied strain and can be quantified by the PD measurement. The details of the fabrication process and the experimental setup are described in the Experimental Section. The strain-response measurement was performed using the human motion detection system (Figure 4b), and it was observed that the sensor shows a high GF (GF ≈ 59) for the uniaxial stretching. It should be noted that many human motions are not just uniaxial stretching but include bending motions. As presented in Figure 4c, the sensor response increased exponentially with the increasing bending angle. To demonstrate the real human motion detection capability, the sensor was integrated on a human finger for detecting the finger-bending motion (Figure 4d and Movie S1). In this graph, it can be observed that the sensor can detect finger-bending motions with good repeatability, stability, and quick response. Moreover, our sensor was utilized for the control of a robot arm with two degrees of freedom (2-DOFs)—a gripper and a wrist. The human finger-bending motion was measured to move the gripper, while the wrist-bending motion was utilized to move the wrist of the robot arm. As shown in Figure 4e and Movie S2, the bending motions of the finger and



https://dx.doi.org/10.1021/acsami.9b18069
ACS Appl. Mater. Interfaces 2020, 12, 10908−10917

wrist were independently transmitted to the robot arm in real-time.

As further wearable sensing applications of our sensor, the posture detection of the neck was carried out. As illustrated in Figure 5a,b, a neck posture sensor module was composed of a multiaxial strain sensor array with an angle of 15° between each sensor (sensor #1, 2, and 3 from the left to the right) and was attached on the backside of the neck. Each sensor showed different output signals by the neck motions. It was observed that the responses increased coincidentally for all three sensors when the backside of the neck extended by forward bending of the neck. When the neck was turned to the left side, the responses of the sensors #2 and #3 increased because tensile strains were applied on them, while the response of the sensor #1 decreased because it was subjected to a compressive loading. As expected, right turning motion of the neck made a opposite consequence. These results show that our sensors could be utilized as a neck posture-monitoring device. Currently, disk disorder is the uprising problems of modern people, which is caused by the wrong position during their working time. The proposed sensor could be a promising solution to prevent this problem by continuous neck posture monitoring.

In addition to the large motion detection explained above, the detection of small motions such as human neck pulse, uvula motion during saliva swallowing, and face motion during speaking or expression can be realized using our sensor. The uniaxial strain sensor was attached on the anterior triangle of the neck where the carotid artery is located (see Figure 6a). The real-time measurement of the carotid pulse was carried out using the sensor (∼70 pulse/min), as shown in Figure 6a. The swallowing motion of the uvula was monitored by our sensor attached on the uvula (Figure 6b). In addition, our sensor was capable to detect the face muscle motion during speaking and emotional face expression changes such as speaking, smiling, and crying that lead to the subtle strain of the skin. Face strain detection when speaking "hello", "yellow", and "red" was carried out, and the result indicated that the sensor could distinguish different face motions by speaking (Figure 6c). When speaking "hello" or "yellow", the sensor showed an increasing response because of the tensile strain applied on the bottom side of orbicularis oris muscle (i.e., muscle between the lips and jaw). When speaking "red", there was an undershoot of the sensor response because of the initial pulsing motion of the lips for pronouncing the "re" sound that applied a compressive strain to the bottom side of orbicularis oris muscle. Similarly, the strain change of the skin below the lips during smiling and crying motions could be detected by our sensor (Figure 6d,e). In summary, the proposed sensor can be applied to the real-time monitoring of various human motions with both subtle strains (neck pulse and face motion) and large strains (neck, finger, and wrist motions).

## CONCLUSIONS

In summary, we developed a novel optical-type strain sensor based on the transmittance change of the CNT-embedded Ecoflex thin film. Tensile strain caused the generation and propagation of microcracks on the CNT network, resulting in the increase in the optical transmittance, which was detected by the photodetector positioned below the CNT-embedded Ecoflex thin film. Our strain sensor shows a wide dynamic range ($\varepsilon = 0$–400%), high sensitivity (GF ≈ 30), small hysteresis (1.8% for $\varepsilon = 0$–100%), and good stability during long-term cyclic loading (drift < 2% for 13,000 cycles of a repeated strain of $\varepsilon = 0$–100%). As compared with the piezoresistive strain sensors, our sensor showed significantly lower hysteresis and higher stability. The sensor has been applied to various wearable human motion-monitoring applications such as the detection of finger-/wrist-bending motions, neck posture, neck pulse, swallowing, and face motion. It is foreseen that our sensor can be broadly applied to the human motion monitoring with a wide range of strains. Furthermore, we believe that the proposed sensor has a great potential for applications in the wearable electronic systems, electronic skins, soft robots, and human–machine interface systems because of its high linearity, quick response, small hysteresis, and superior long-term stability.

## ASSOCIATED CONTENT

### Supporting Information

The Supporting Information is available free of charge at https://pubs.acs.org/doi/10.1021/acsami.9b18069.

Sensitivity tuning factor analysis; independency of the sensor response to the intensity of the light source; additional sensor characteristics; comparison of the performances of the sensor with other nanofiller-based strain sensors; details of the fabrication process; experimental setup; and image analysis process (PDF)

Real-time monitoring of the finger bending using the CNT-embedded thin film-based strain sensor (AVI)

Control of robot motions using a real-time monitoring of the human finger and wrist motions (AVI)

## AUTHOR INFORMATION


### Corresponding Author

**Inkyu Park** − *Department of Mechanical Engineering, Korea Advanced Institute of Science and Technology (KAIST), Daejeon 305-701, South Korea;* orcid.org/0000-0001-5761-7739; Email: inkyu@kaist.ac.kr

### Authors

**Jimin Gu** − *Department of Mechanical Engineering, Korea Advanced Institute of Science and Technology (KAIST), Daejeon 305-701, South Korea*

**Donguk Kwon** − *Package Process Development Team Samsung Electronics, Asan-si, South Korea*

**Junseong Ahn** − *Department of Mechanical Engineering, Korea Advanced Institute of Science and Technology (KAIST), Daejeon 305-701, South Korea*

Complete contact information is available at: https://pubs.acs.org/10.1021/acsami.9b18069


### Author Contributions

The manuscript was written through contributions of all authors. All authors have given approval to the final version of the manuscript.


### Funding

This work was supported by the National Research Foundation of Korea (NRF) grant funded by the Korea government (MSIT) (no. 2018R1A2B2004910). This work was also supported by the National Research Foundation of Korea (NRF) Grant funded by the Korean Government (MSIP) (no. 2015R1A5A1037668).


### Notes

The authors declare no competing financial interest.

## REFERENCES


(1) Kim, J.; Lee, J.; Son, D.; Choi, M. K.; Kim, D.-H. Deformable Devices with Integrated Functional Nanomaterials for Wearable Electronics. *Nano Convergence* **2016**, *3*, 1−13.

(2) Trung, T. Q.; Lee, N.-E. Flexible and Stretchable Physical Sensor Integrated Platforms for Wearable Human-Activity Monitoringand Personal Healthcare. *Adv. Mater.* **2016**, *28*, 4338−4372.

(3) Amjadi, M.; Kyung, K.-U.; Park, I.; Sitti, M. Stretchable, Skin-Mountable, and Wearable Strain Sensors and Their Potential Applications: A Review. *Adv. Funct. Mater.* **2016**, *26*, 1678−1698.

(4) Kenry; Yeo, J. C.; Lim, C. T. Emerging Flexible and Wearable Physical Sensing Platforms for Healthcare and Biomedical Applications. *Microsyst. Nanoeng.* **2016**, *2*, 16043.

(5) Nag, A.; Mukhopadhyay, S. C.; Kosel, J. Wearable Flexible Sensors: A Review. *IEEE Sens. J.* **2017**, *17*, 3949−3960.

(6) Pang, C.; Lee, C.; Suh, K.-Y. Recent Advances in Flexible Sensors for Wearable and Implantable Devices. *J. Appl. Polym. Sci.* **2013**, *130*, 1429−1441.

(7) Lee, W. S.; Jeon, S.; Oh, S. J. Wearable Sensors Based on Colloidal Nanocrystals. *Nano Convergence* **2019**, *6*, 10.

(8) Amjadi, M.; Pichitpajongkit, A.; Lee, S.; Ryu, S.; Park, I. Highly Stretchable and Sensitive Strain Sensor Based on Silver-Elastomer Nanocomposite. *ACS Nano* **2014**, *8*, 5154−5163.

(9) Lee, S.; Shin, S.; Lee, S.; Seo, J.; Lee, J.; Son, S.; Cho, H. J.; Algadi, H.; Al-Sayari, S.; Kim, D. E.; et al. Ag Nanowire Reinforced Highly Stretchable Conductive Fibers for Wearable Electronics. *Adv. Funct. Mater.* **2015**, *25*, 3114−3121.

(10) Yao, S.; Zhu, Y. Wearable Multifunctional Sensors Using Printed Stretchable Conductors Made of Silver Nanowires. *Nanoscale* **2014**, *6*, 2345−2352.

(11) Lee, J.; Kim, S.; Lee, J.; Yang, D.; Park, B. C.; Ryu, S.; Park, I. A Stretchable Strain Sensor Based on a Metal Nanoparticle Thin Film for Human Motion Detection. *Nanoscale* **2014**, *6*, 11932−11939.

(12) Yang, Z.; Wang, D.-Y.; Pang, Y.; Li, Y.-X.; Wang, Q.; Zhang, T.-Y.; Wang, J.-B.; Liu, X.; Yang, Y.-Y.; Jian, J.-M.; et al. Simultaneously Detecting Subtle and Intensive Human Motions Based on a Silver Nanoparticles Bridged Graphene Strain Sensor. *ACS Appl. Mater. Interfaces* **2018**, *10*, 3948−3954.

(13) Wang, Y.; Wang, L.; Yang, T.; Li, X.; Zang, X.; Zhu, M.; Wang, K.; Wu, D.; Zhu, H. Wearable and Highly Sensitive Graphene Strain Sensors for Human Motion Monitoring. *Adv. Funct. Mater.* **2014**, *24*, 4666−4670.

(14) Pang, Y.; Tian, H.; Tao, L.; Li, Y.; Wang, X.; Deng, N.; Yang, Y.; Ren, T.-L. Flexible, Highly Sensitive, and Wearable Pressure and Strain Sensors with Graphene Porous Network Structure. *ACS Appl. Mater. Interfaces* **2016**, *8*, 26458−26462.

(15) Amjadi, M.; Yoon, Y. J.; Park, I. Ultra-Stretchable and Skin-Mountable Strain Sensors Using Carbon Nanotubes-Ecoflex Nanocomposites. *Nanotechnology* **2015**, *26*, 375501.

(16) Kanoun, O.; Müller, C.; Benchirouf, A.; Sanli, A.; Dinh, T.; Al-Hamry, A.; Bu, L.; Gerlach, C.; Bouhamed, A. Flexible Carbon Nanotube Films for High Performance Strain Sensors. *Sensors* **2014**, *14*, 10042−10071.

(17) Lee, D.; Hong, H. P.; Lee, C. J.; Park, C. W.; Min, N. K. Microfabrication and Characterization of Spray-Coated Single-Wall Carbon Nanotube Film Strain Gauges. *Nanotechnology* **2011**, *22*, 455301.

(18) Zhou, J.; Yu, H.; Xu, X.; Han, F.; Lubineau, G. Ultrasensitive, Stretchable Strain Sensors Based on Fragmented Carbon Nanotube Papers. *ACS Appl. Mater. Interfaces* **2017**, *9*, 4835−4842.

(19) Hu, N.; Itoi, T.; Akagi, T.; Kojima, T.; Xue, J.; Yan, C.; Atobe, S.; Fukunaga, H.; Yuan, W.; Ning, H.; et al. Ultrasensitive Strain Sensors Made from Metal-Coated Carbon Nanofiller/Epoxy Composites. *Carbon* **2013**, *51*, 202−212.

(20) Lee, H.; Kwon, D.; Cho, H.; Park, I.; Kim, J. Soft Nanocomposite Based Multi-Point, Multi-Directional Strain Mapping Sensor Using Anisotropic Electrical Impedance Tomography. *Sci. Rep.* **2017**, *7*, 39837.

(21) Parmar, K.; Mahmoodi, M.; Park, C.; Park, S. S. Effect of CNT Alignment on the Strain Sensing Capability of Carbon Nanotube Composites. *Smart Mater. Struct.* **2013**, *22*, 075006.

(22) Cai, L.; Song, L.; Luan, P.; Zhang, Q.; Zhang, N.; Gao, Q.; Zhao, D.; Zhang, X.; Tu, M.; Yang, F.; et al. Super-Stretchable, Transparent Carbon Nanotube-Based Capacitive Strain Sensors for Human Motion Detection. *Sci. Rep.* **2013**, *3*, 3048.

(23) Lee, J.; Lim, M.; Yoon, J.; Kim, M. S.; Choi, B.; Kim, D. M.; Kim, D. H.; Park, I.; Choi, S.-J. Transparent, Flexible Strain Sensor Based on a Solution-Processed Carbon Nanotube Network. *ACS Appl. Mater. Interfaces* **2017**, *9*, 26279−26285.

(24) Tang, Z.; Jia, S.; Wang, F.; Bian, C.; Chen, Y.; Wang, Y.; Li, B. Highly Stretchable Core-Sheath Fibers via Wet-Spinning for Wearable Strain Sensors. *ACS Appl. Mater. Interfaces* **2018**, *10*, 6624−6635.

(25) Tang, Z.; Jia, S.; Shi, S.; Wang, F.; Li, B. Coaxial Carbon Nanotube/Polymer Fibers as Wearable Piezoresistive Sensors. *Sens. Actuators, A* **2018**, *284*, 85−95.

(26) Zhang, S.; Wen, L.; Wang, H.; Zhu, K.; Zhang, M. Vertical CNT-Ecoflex Nanofins for Highly Linear Broad-Range-Detection Wearable Strain Sensors. *J. Mater. Chem. C* **2018**, *6*, 5132−5139.

(27) Zhai, Q.; Yang, Y. Highly Stretchable Variable-Transmittance Skin for Ultrasensitive and Wearable Strain Sensing. *Adv. Mater. Technol.* **2017**, *2*, 1700161.

(28) Deng, F.; Ito, M.; Noguchi, T.; Wang, L.; Ueki, H.; Niihara, K.-i.; Kim, Y. A.; Endo, M.; Zheng, Q.-S. Elucidation of the Reinforcing Mechanism in Carbon Nanotube/Rubber Nanocomposites. *ACS Nano* **2011**, *5*, 3858−3866.

(29) Ponnamma, D.; Sadasivuni, K. K.; Grohens, Y.; Guo, Q.; Thomas, S. Carbon Nanotube Based Elastomer Composites-an Approach towards Multifunctional Materials. *J. Mater. Chem. C* **2014**, *2*, 8446−8485.

(30) Kim, H.-i.; Wang, M.; Lee, S. K.; Kang, J.; Nam, J.-D.; Ci, L.; Suhr, J. Tensile Properties of Millimeter-Long Multi-Walled Carbon Nanotubes. *Sci. Rep.* **2017**, *7*, 9512.

(31) Qiu, A.; Li, P.; Yang, Z.; Yao, Y.; Lee, I.; Ma, J. A Path Beyond Metal and Silicon:Polymer/Nanomaterial Composites for Stretchable Strain Sensors. *Adv. Funct. Mater.* **2019**, *29*, 1806306.

(32) Shrivastava, A.; Gupta, V. Methods for the Determination of Limit of Detection and Limit of Quantitation of the Analytical Methods. *Chron. Young Sci.* **2011**, *2*, 21.

(33) Lee, T.-I.; Kim, M. S.; Kim, T.-S. Contact-Free Thermal Expansion Measurement of Very Soft Elastomers Using Digital Image Correlation. *Polym. Test.* **2016**, *51*, 181−189.

(34) Cohen, D. J.; Mitra, D.; Peterson, K.; Maharbiz, M. M. A Highly Elastic, Capacitive Strain Gauge Based on Percolating Nanotube Networks. *Nano Lett.* **2012**, *12*, 1821−1825.

(35) Kim, K.-H.; Jang, N.-S.; Ha, S.-H.; Cho, J. H.; Kim, J.-M. Highly Sensitive and Stretchable Resistive Strain Sensors Based on Microstructured Metal Nanowire/Elastomer Composite Films. *Small* **2018**, *14*, 1704232.

(36) Liao, X.; Zhang, Z.; Kang, Z.; Gao, F.; Liao, Q.; Zhang, Y. Ultrasensitive and Stretchable Resistive Strain Sensors Designed for Wearable Electronics. *Mater. Horiz.* **2017**, *4*, 502−510.

(37) Li, X.; Zhang, R.; Yu, W.; Wang, K.; Wei, J.; Wu, D.; Cao, A.; Li, Z.; Cheng, Y.; Zheng, Q.; et al. Stretchable and Highly Sensitive Graphene-on-Polymer Strain Sensors. *Sci. Rep.* **2012**, *2*, 870.

(38) Yu, X.-G.; Li, Y.-Q.; Zhu, W.-B.; Huang, P.; Wang, T.-T.; Hu, N.; Fu, S.-Y. A Wearable Strain Sensor Based on a Carbonized Nano-Sponge/Silicone Composite for Human Motion Detection. *Nanoscale* **2017**, *9*, 6680−6685.




https://dx.doi.org/10.1021/acsami.9b18069
ACS Appl. Mater. Interfaces 2020, 12, 10908−10917